Chapter 11

Nanoindentation of Human Trabecular Bone – Tissue Mechanical Properties Compared to Standard Engineering Test Methods

Ondřej Jiroušek

Additional information is available at the end of the chapter

http://dx.doi.org/10.5772/50152

1. Introduction

There are generally two types of bone tissue: trabecular and cortical. Cortical bone is the more dense tissue found on the surface of bones and trabecular bone is a highly porous structure that fills the proximal and distal ends of all long bones (e.g. femur or tibia) and is also present as a filler in other bones (e.g. in vertebral bodies). While at the molecular level both the cortical and trabecular bone are made of the same constituents, their overall mechanical properties are quite different.

Material properties of trabecular bone bone are influenced not only by the architecture and connectivity of individual trabeculae, but also by the properties at the molecular level. At this level one can consider bone to be a composite mineral consisting of organic and inorganic constituents. To relate the overall mechanical properties (strength, stiffness, yield properties) to its microstructure, it is necessary to measure the properties of individual trabeculae. One has to bear in mind the very small dimensions of single trabecula. Although the trabecular microstructure is dependent on the anatomical site, the typical length of trabecula is 1-2 mm with diameter around 100 microns. This makes assessment of mechanical properties at the level of single trabeculae quite a challenging task.

To measure the mechanical properties of trabecular bone at the tissue level (at the level of individual trabeculae) five main methods has been designed and used: (i) tensile or three- (four-) point bending tests, (ii) buckling studies, (iii) acoustic methods, (iv) back-calculation from finite element simulations, (v) nanoindentation. There is a significant scatter in the material properties obtained by any of these methods, even when the same method is used by different authors. The published mechanical properties of human trabecular bone vary between 1 GPa and 15 GPa. The cause of this broad discrepancy in results might be in sample preparation, different testing protocols or anisotropy and asymmetry of the micro-samples. In this chapter, two most favorite methods (nanoindentation and micromechanical testing) will be compared.

2. Composition and structure of bone

At the *molecular* level, bone is a composite material made of collagen matrix stiffened by crystalline salts composed primarily of calcium and phosphate. Collagen is a fibrous protein found in flesh and connective tissues. It is a soft organic material and the main structural protein in the human body. The collagen provides the bone with toughness, while the rigidity and stiffness of the bone is provided by inorganic salts. Apart from collagen, other proteins are present in the bone. These include glycoproteins and protein-polysacharides ("proteoglycans") which create an amorphous mixture of extracellular material.

These proteins comprise about 30–50% of the bone volume. In addition to this protein constituent of bone, there is the inorganic constituent – a mineral very similar to hydroxyapatite, which is a naturally occurring mineral form of calcium apatite and can be described chemically as $Ca_{10}(PO_4)_6(OH)_2$. Hydroxyapatite in bone includes calcium phosphate, calcium carbonate, calcium fluoride, calcium hydroxide and citrate. In bone, the mineral is present in form of crystals with the shape of plates or rods, with thickness about 8 to 15 Å, width 20 to 40 Å and length 200 to 400 Å.

To summarize, on molecular level bone is a *hard* or *mineralized* or *calcified* tissue, consisting from organic matrix impregnated with the inorganic bone mineral. About 70% of the bone weight is given by the inorganic mineral. Generally, bone mineral shows positive correlation with bone strength, however, in metabolic diseases, such osteoporosis it fails to predict the bone strength correctly because these metabolic disorder results in weaker bones in presence of greater mineral density.

Going from the *molecular* level up, one can see that the collagen molecules and crystals of hydroxyapatite are assembled into microfibrils. These fibrils are again assembled into fibers with thickness about 3 to 5 µm. This level is often called *ultrastructural* level. The next level is important from the material properties point of view. In this level, the fibers are assembled either randomly into *woven* bone or are organized into lamellae forming *lamellar* bone. These lamellae can be either in concentric groups, called osteons or can form linear lammelar groups, called *plexiform* bone. This level is called *microstructural* level.

At the same level, the bone is different not only in terms of lamellar organization, but also in terms of its architectural organization. There are two types of architectural structure present in all types of bones. On the surface of the bones, there is a thin layer of dense bone, called *cortical* or *compact* bone. Under this dense layer the ends of all weight-bearing bones are filled with less dense type of bone, called *trabecular* or *spongional* bone (see Fig. 1). The primary function of the cortical bone is to support the whole body, to provide for the movement and to protect the soft inner organs. Secondary function of the cortical bone is to store and release calcium.

The trabecular bone gives supporting strength to the ends of long bones, vertebral bodies and other bones providing structural support and flexibility. The inner structure of trabecular bone is a result of structural optimization provided by remodeling processes. Result of these processes is a strong, but lightweight structure with superior mechanical properties without the weight of compact bone.

From the above mentioned arises the importance of the bone composition and structure at molecular, ultrastructural and microstructural levels for the resulting mechanical properties

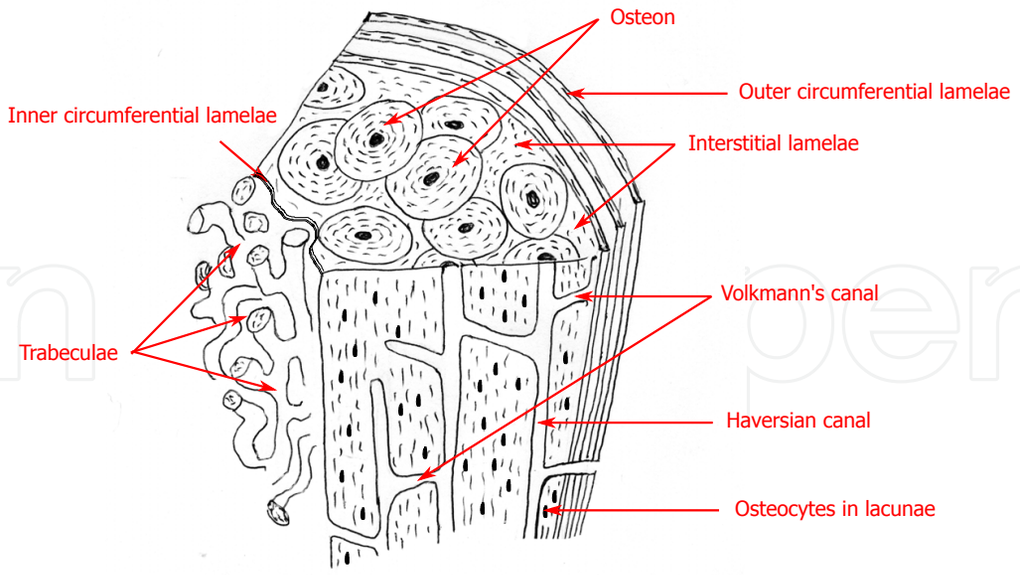

Figure 1. A schematic picture of bone structure showing trabecular, lamellar and cortical bone. Interstitial and circumferential (inner and outer) lamelae are distinguished.

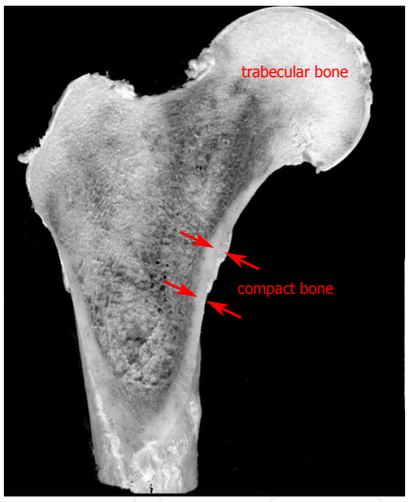

Figure 2. Longitudinal cut through proximal part of human femur. Red arrows indicate the thickness of cortical bone layer.

of both cortical and trabecular bone. And because in the living organism the skeleton is a metabolically active organ undergoing continuous remodeling process one has to distinguish between the newly deposited bone and fully calcified (old) bone. Bone remodeling is a lifelong process composed of *resorption* (old bone tissue removal) and *formation* (aposition of new bone). For the trabecular bone, most of the remodeling process takes place on the surface of the trabecular structure, the interstitial bone (bone tissue in the middle part of trabeculae) is often excluded from remodeling [1, 2]. This phenomenon has a consequence in highly nonuniform distribution of mineral content [3]. In the new bone tissue, most of the mineral is deposited in a couple of days (approximately 70%), then the process slows down dramatically and the remaining mineral is deposited in the following years [4]. Thus, the interstitial bone has a larger mineral content compared to the bone on the surface.

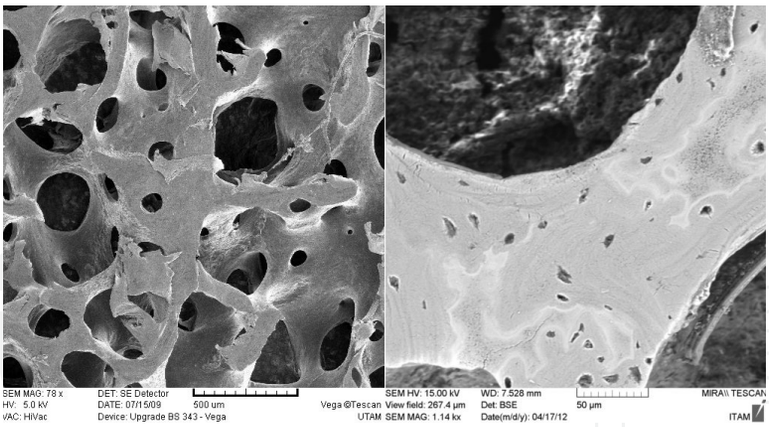

Figure 3. Trabecular bone as seen in scanning electron microscope (SEM). Sample of healthy bone from human proximal femur. The dark dots in the enlarged image are lacunae that contain osteocytes (most numerous bone cell).

2.1. Bone quality assessment

Traditionally, bone quality is described by bone mass or Bone Mineral Density (BMD) measured by dual energy X-ray absorptiometry (DXA, previously DEXA) [5], [6]. Today, BMD is used as a predictor of fracture risk in both healthy and osteoporotic bone. In DXA measurements, two X-ray beams with different energy levels are used and the absorption of X-rays by the tissues is measured. The two distinct energy levels allows to differentiate the bone tissue from the soft tissues (one X-ray beam is absorbed mainly by the soft tissues). The BMD is evaluated after the X-ray absorption by the soft tissues is eliminated.

One of the reasons for DXA failing to assess the risk of osteoporotic fracture properly [7] is the fact that bone mechanical properties correlate not only to the bone mineral density, but more importantly to its three-dimensional inner structure [8, 9]. Moreover, recent studies, e.g. [10] show the inability of DXA to account for the large variability in skeletal size and body composition in growing children.

Proper, precise and reliable assessment of morphometric and mechanical properties of trabecular bone have both biological and clinical importance. Fracture risk assessment at early time is essential for better treatment of bone diseases such as osteoporosis. To improve the reliability of fracture risk assessment, it is necessary to improve the diagnostic possibilities of modern imaging systems, such as microfocus computed tomography (micro-CT) or high-resolution peripheral quantitative computed tomography (HR-pQCT) for assessment of the 3D microstructure of cortical and trabecular bone in vivo and to improve measurement techniques to assess the material properties of trabecular (and cortical) bone at the microstructural level.

2.2. Measurement of bone mechanical properties

Mechanical properties of engineering materials are usually measured experimentally by performing mechanical tests. For engineering materials a sample of the material of known dimensions is prepared and exposed to mechanical load to measure its strength, elastic constants or other material properties under various loading and environmental conditions. For engineering materials there is a set of standardized test methods such as those developed by the American Society for Testing and Materials (ASTM) and the International Organization

for Standardization (ISO). However, testing of biological materials is more complicated – often it is not possible to prepare a sample with specific dimensions and, more importantly, because the capability of the tissue to retain its natural material properties ex vivo is limited, environmental conditions, namely temperature and hydration must be considered during the tests.

Most of the tissues exhibit viscoelastic or viscoplastic behavior. This is highlighted in soft tissues, such as ligaments and tendons, but to some extent it is characteristic for all tissues. Mechanical properties of trabecular bone are inhomogeneous or site-specific, i.e. they depend on position in the material [11]. Moreover, they are dependent on anatomic location [12], e.g. Young's modulus of trabecular bone from femoral head is different from vertebral body. They are non-linearly viscoelastic [13] and display anisotropic behavior, which is usually described as orthotropic [14]. The orthotropic behavior of trabecular bone is given by the microstructural arrangement of the trabecular network; at the level of single trabecula the properties can be considered isotropic. The only study that studies the anisotropy in elastic properties of trabecular bone is [15] in which the authors used microindentation with depth equal to 2.5 μm in six different regions of interest – three on axial and three on transverse sections through trabeculae. In axial direction the bone exhibit significantly higher indentation modulus than in transverse direction, suggesting the transverse anisotropy for vertebral trabecular bone. However, there is no other study proving the anisotropy of indentation modulus for trabecular bone. This is in contrary to the compact bone where the anisotropy is present at different level of detail, i.e. single osteon is anisotropic [16] with a higher stiffness value aligned along the axial direction.

As already mentioned, experimental conditions, especially temperature and water content are influencing the results of bone mechanical testing [17]. Generally, bone stiffness increases slightly with decreasing temperature. Higher temperature has a consequence in collagen denaturation which leads to a significant decrease in the toughness of bone, but the effect on the stiffness of bone is low [18]. Effects of hydration were studied both at the microlevel, for instance in [19] nanoindentation creep tests were used for quantification of elastic and viscoelastic properties as a function of water content, or at the macrolevel, e.g. in [20] the authors studied the effect of dehydration and rehydration on the flexural properties of whole bones (mouse femora). Generally speaking, hydration increase is associated with significant (up to $\sim$40%) decrease in bone stiffness [21] and elastic properties are regained at different rates. The change in bone properties due to the dehydration can be overcome by some methods that are able to prevent the loss of hydration. Usually, the samples are tested in a phosphate-buffered saline (PBS) bath or the PBS is dripped on its surface during the experiment.

From the aforementioned complexity of material properties of trabecular bone it is evident that great care must be paid to proper sample preparation, handling during the experiment and keeping stable environmental conditions. There is a great potential of incorrectness in existing testing procedures and one must be aware of all possible error sources. Both methods, that will be discussed – nanoindentation and micromechanical testing – have their advantages and disadvantages. While micromechanical tests are more straightforward, the sample extraction, handling and measurement of the deformation is very demanding. On the other hand, nanoindentaion of a block of trabecular bone has its own limitations, not only due to difficulties in preserving the bone natural properties, but due to other effects which will be described in the following section.

3. Nanoindentation of trabecular bone

Nanoindentation measures the Young's modulus of small-volume samples with the help of a diamond tip pressed in the polished surface of the sample while the applied force and indentation depth are measured. The depth sensing indentation methods have been developed because of the difficulty in precise measurement of the contact area between the sample and the diamond tip. These methods record continuously the displacement of the tip and the contact area is calculated from the known geometry of the tip and the indentation depth.

Today, the most used model for nanoindentation is a model developed by Oliver and Pharr [22, 23] which calculates elastic properties from the unloading part of the indentation curve. This approach assumes that the unloading is purely elastic and the contact can be therefore treated as Hertzian. It has been proved that the technique is valid for axisymmetric indenters with infinitely smooth profile [22, 24] though it assumes at least four simplifying assumptions: i) perfect geometry of the indenter, ii) zero adhesive and frictional forces, iii) specimen is treated as infinite half-space and iv) material is linear elastic and incompressible.

Since in the Oliver and Pharr method an elastic contact analysis is used, only elastic properties of the material can be directly obtained. Another approach is to use finite element (FE) simulation of the contact in which various aspects of the contact, e.g. the three-dimensional nature, nonlinear material properties, time effects, can be treated. First FE studies of nanoindentation were those of Dumas [25] and Hardy [26], later studies focused on various aspects of the indentation problem, e.g. on plasticity [27]. Parameters of advanced material models can be ascertained by fitting the experimental load–displacement curves to curves obtained from the FE simulations [28, 29].

Early studies on bone nanoindentation showed great variability of measured elastic properties obtained from specimens from different anatomical locations [30, 31], although there were also few studies concluding that at the tissue level, elastic properties of trabecular and cortical bone are similar, e.g. [32]. Statistically significant difference in elastic properties and hardness of microstructural components of cortical bone, individual trabeculae and interstitial lamellae has been shown by Rho in [30]. It was shown by Zysset in [31] that hardness and elastic modulus differ substantially among lamellar types, anatomical sites and individuals. Authors suggested that tissue heterogeneity plays an important role in bone fragility and adaptation. Dependence of the elastic moduli on the direction was shown also by Rho et al. [33] resulting in larger elastic moduli in the longitudinal direction than in the transverse. Variability in bone mechanical properties dependent on anatomical site has been proven for diaphyseal and metaphyseal parts, showing greater elastic modulus and hardness for diaphyseal than metaphyseal tissues [34] confirming that tissue properties vary with anatomical location and may reflect differences in the average tissue age or mineral and collagen organization. This heterogeneity in elastic moduli of human bone at the lamellar level was observed also by other authors [35]. For compact bone, it is therefore important to distinguish between the osteonal, interstitial, and lamellar tissue which all have higher elastic moduli than trabecular bone from the same anatomical location.

These effects can be explained by a characteristic bone mineralization density distribution (BMDD) which describes local mineral content (calcium concentrations) in the (heterogeneously mineralized) bone matrix [36]. BMDD is a measure of bone matrix mineralization and compared to BMD is a more local measure for the amount of bone

mineral. Combined with nanoindentation, BMDD measurements can provide important information about the structure-function relationship and explain the above-mentioned great variability in local mechanical properties of bone.

It is evident, that precise measurement of local mechanical properties is of key interest for proper description of bone mechanics. For cortical bone, it is required to measure the elastic modulus and hardness at the level of individual osteons, whereas for trabecular bone it is important to distinguish between individual trabeculae and to account for the cross-sectional difference. The only study that uses nanoindentation of individual trabeculae in their cross-sections is the study by Brennan el al. [39], however, the properties were measured only in three distinct areas (core, middle, outer) and the authors used quasi-static nanoindentation. Another possibility to measure variations in material properties in the cross-section of trabecula is to use modulus mapping (MM) [40]. Both techniques will be discussed in the following paragraphs.

3.1. Sample preparation techniques

Results of nanoindentation are highly influenced by the sample preparation procedure. This is especially true for biological tissue samples due to the difficulty of sample fixation. It is well-known both for compact and trabecular bone, that hardness and elastic modulae are dependent on the water content, resulting in up to 40% difference in measured indentation modulus [21]. For wet conditions the indentation modulus decreases.

Because the intention of this study was to compare different techniques to assess the bone properties and because the compared methods (nanoindentation and micromechanical testing) are time-consuming all the samples were tested in dry conditions. The water promotes enzymatic degradation of the bone collagen matrix and because the nanoindentation experiments with large set of different parameters take hours it would be very difficult to maintain stable conditions during the experiment. For this reason all tested samples were dried in stable conditions (48 hours at 40°C) prior the experiments. The author is aware of the fact, that revealed stiffness is higher than stiffness of the bone tested under wet conditions.

Optimizing of the sample preparation process was presented by Dudikova et al in [41]. Different approaches are described and results of the selected surface preparation procedures compared. Effects of the grain size, load and duration time of grinding on surface roughness are analyzed using confocal laser scanning microscopy. Monitoring and optimization of roughness reduction procedure used for preparation of samples for nanoindentation tests was compared to evaluate the optimal forces and times of grinding. The most suitable procedure with respect to time and cost was proposed.

3.2. Quasi-static nanoindentation of trabecular bone

The standard compliance method by Oliver and Pharr assumes elastic, isotropic materials with negligible adhesion. Bone and other tissues exhibit viscoelastic or time-dependent behavior. The viscoelastic behavior has a consequence in the nanoindentation tip sinking in the material's surface under constant load (creep). This creep behavior is observed in the force–displacement curve as a 'nose' in the unloading part. To avoid this effect (slope of the unloading part is used for calculation of the Young's modulus in the compliance method) a hold period when the maximum load is kept constant for 3-120 s is introduced to allow

the creep to diminish prior unloading. The issue of removing the creep effect from the contact-depth and contact-area measurement using the trapezoidal load function (see Fig. 5) during nanoindentation is addressed in [42]. Introducing holding period to the loading function for the minimization of the creep effects on evaluated elastic properties is widely used also for other types of viscoelastic materials ranging from polymers to cementitious composites, see e.g. [43–45].

To illustrate the quasi-static nanoindentation of trabecular bone a detailed experimental procedure will be described. To measure material properties of trabecular bone in human proximal femur a set of different indentation experiments was undertaken using a small cubic sample of bone tissue obtained from embalmed cadaver (male, 72 year) using a diamond blade saw (Isomet 2100, Buehler Ltd., USA). The fat and marrow was removed from the sample using a soft water jet followed by repetitive ultrasonic cleaning. The sample was fixed in a low shrinkage epoxy resin and polished with diamond discs of grain size 35 and 15 µm. The surface was finished with monocrystalline diamond suspension of grain size 9, 3 and 1 µm. For the final polishing aluminum-oxide Al_2O_3 suspension with grain size 0.05 µm on a soft cloth was used.

Prior the mechanical testing the surface roughness of the sample was measured in a confocal laser scanning microscope (Lext OLS3000, Olympus America Inc., USA). The peak roughness R_p (the highest peak in the roughness profile) of the finished surface was 15 nm. The sample was then fixed in nanoindenter and indented using two different peak forces, 10 mN and 20 mN. For both peak forces a grid of 20 indents was performed with different set of parameters. Apart from the two peak forces, three different loading rates were used (20, 120, 240 mN/min) and three different holding times (10, 20, 40 s).

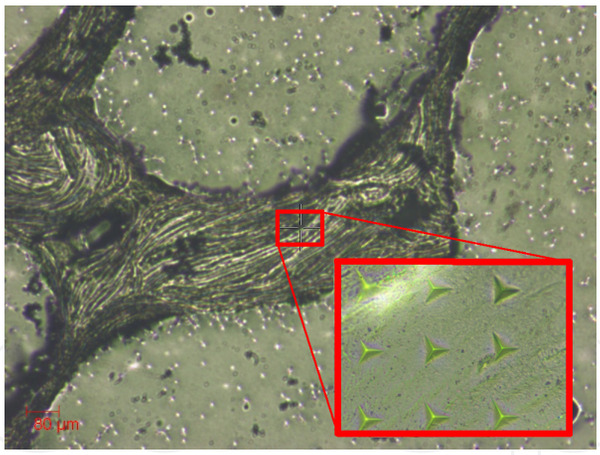

Figure 4. Sample trabecula with places of indents (Berkovich indenter)

Berkovich tip (a three sided pyramid) was used in the experiments. The indents were made with 10 µm grid size (see Fig. 4). For each indent force-depth curves were plotted and hardness and modulae of elasticity were calculated for each nanoindentation curve with the Oliver-Pharr method [22]:

$$\frac{1}{E_r} = \frac{1-\nu^2}{E} + \frac{1-\nu_i^2}{E_i} \tag{1}$$

where E_i , ν_i is Young's modulus and Poisson's ratio of the diamond tip. E, ν is Young's modulus and Poisson's ratio of the tested material (bone). In this study, Poisson's ration of the

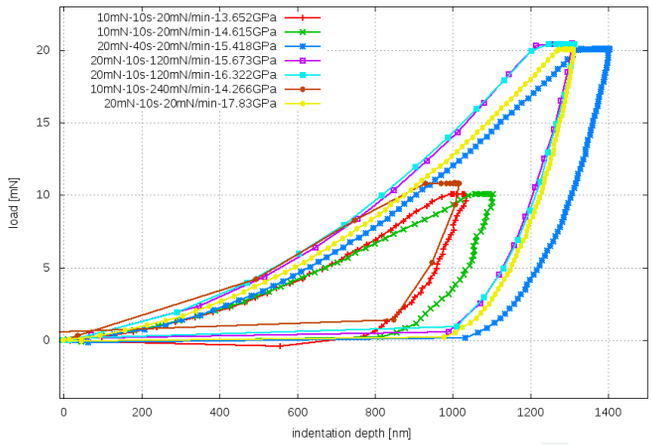

Figure 5. Set of nanoindentation curves measured with different peak forces and velocities.

	Dwell time [s]				
peak force [mN]	1.25	2.5	5	10	30
10	13.04±0.63	10.58±0.48	11.80±0.60	11.43±0.99	13.23±0.39
20	15.34±1.71	14.22±0.94	15.75±1.19	14.46±1.30	14.21±1.67

Table 1. Young's modulus from nanoindentation using different hold times for two maximum indentation forces.

sample ν was taken from our tensile experiments with single trabeculae. Reduced modulus E_r is calculated from following equation introduced by Sneddon [46]:

$$E_r = \frac{\sqrt{\pi}}{2}\frac{S}{\sqrt{A}},\ S = \frac{dP}{dh} \tag{2}$$

where A is the projected area of elastic contact, S is the contact stiffness (experimentally measured from the unloading data).

In average, there were 17 successful indents in each set of parameters. Obtained values of Young's modulus for selected indentation curves (see Fig. 5) for different holding times that were later used in the inverse FE calculations are shown in the Tab. 1.

3.3. Inverse calculation of material parameters from FE model of nanoindentation

The previously presented derivation of material properties from nanoindetation experiment is based on linear elastic assumptions, i.e. while the loading stage is elasto-plastic, the unloading stage is purely elastic. Young's modulus of elasticity of the indented material was derived from the unloading curve. Using the Oliver-Pharr method only elastic material constants can be derived directly from the measurements. However, two nonlinear phenomena are present in the nanoindentation problem: i) contact with friction between the indenter and material's surface, and ii) elasto-plasticity of the tested material. Because it is not possible to derive analytical solution for this problem a numerical modeling using approximate solution of the complex problem must be used. Usually, finite element method is used to obtain the approximate solution. This part shortly describes a "numerical experiment" performed to establish the parameters of a material model for trabecular bone.

The indentation problem was modeled as rotationally axisymmetric problem in which the Bercovich pyramidal indenter was replaced with equivalent cone. The sharp tip of the cone was rounded due to the use of nonlinear contact between indenter and specimen. For better numerical convergence the sharp tip of the cone is usually rounded $100 \sim 300$ nm. In the presented model, radius r =200 nm was chosen. The FE model (see Fig. 6) was composed from 13,806 2-D structural solid elements (6,997 nodes) with linear shape functions. Between the indenter and the surface of the material frictionless contact was modeled.

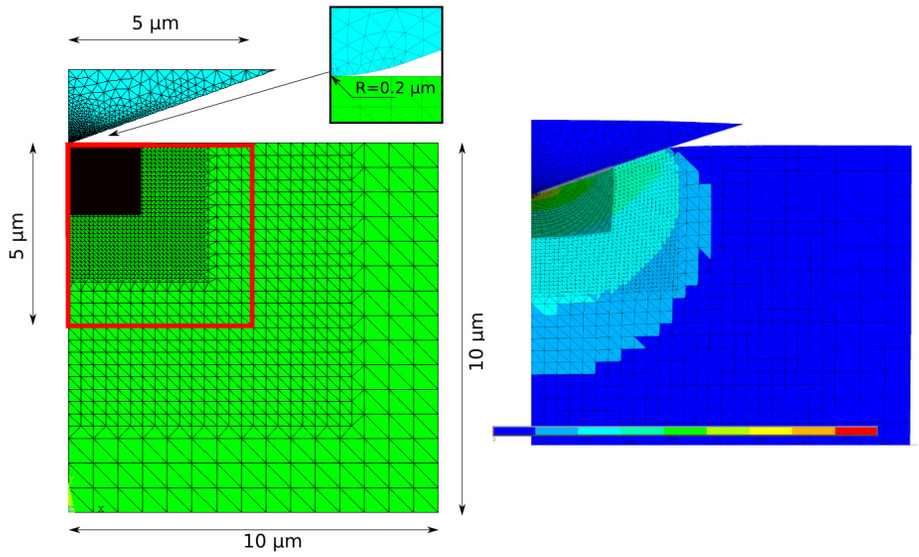

Figure 6. Axisymmetric FE model of nanoindentation experiment used for back-calculation of parameters of material model (elasto-plastic with kinematic hardening)

For the diamond nanoindenter elastic material model (E_i=1140 GPa, μ_i=0.2) was used. The trabecular bone was modelled using elasto-plastic material model with two different yield criteria – von Mises yield criterion and pressure-dependent Drucker-Prager yield condition. Bilinear isotropic hardening was chosen for both considered models. In case of von Mises plasticity with kinematic hardening rule, four material constants are needed for complete description, Young's modulus E, Poisson's ratio ν, yield stress σ_y and tangent modulus E_{tan}. Since the Drucker-Prager model is a smooth version of the Mohr–Coulomb yield surface, it is usually expressed in terms of the cohesion d, angle of internal friction φ and dilatation angle. Therefore the model is given by five constants: Young's modulus E, Poisson's ratio ν, cohesion d, friction angle φ and dilatation angle θ.

In both considered models, Young's modulus and Poisson's ratio were taken from the nanoindentation experiment. Remaining material constants ($\langle \sigma_y,\ E_{tan} \rangle$ or $\langle d,\ \varphi,\ \theta \rangle$) were evaluated by fitting the nanoindentation curves.

The set of nanoindentation curves with different load speeds, holding times and maximal forces was sampled using linear approximation. Values of force and penetration depth at approximation points were calculated for each nanoindentation curve. The indenter was loaded incrementally with force values in each load step of the FE simulation (450 load steps per simulation). A least-squares approach was used to compare the experimental force-penetration depth curves with curves obtained from each FE simulation with one set of material parameters. Flowchart of the fitting procedure is schematically shown in Fig. 7.

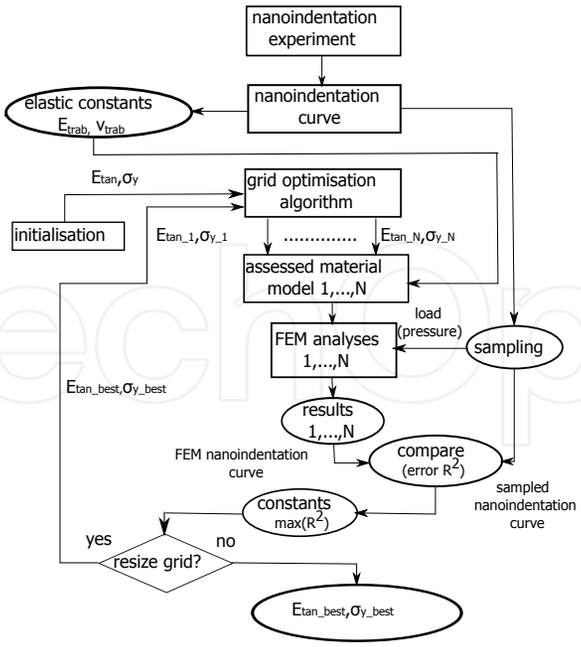

Figure 7. Flowchart of the procedure used to establish the parameters of elasto-plastic material model by fitting the nanoindentation curves from FEA to experimental curves.

Axisymmetric FE model was loaded according to the experiment using prescribed boundary conditions. A convergence study was performed to ensure the sufficient mesh density. Results from the least square fitting obtained both for the von Mises and Drucker-Prager plasticity criterion for one selected case (peak force 10 mN, holding time 5 s) are shown in Tab. 2. The fitting procedure was undertaken for every set of indentation parameters (maximal force, loading rate, dwell time).

Model	E [GPa]	ν	σ_y [MPa]	E_{tan} [MPa]	d [MPa]	$\beta[^\circ]$	$\psi[^\circ]$
von Mises	11.4	0.2	92	1420	–	–	–
D-P	11.4	0.2	–	–	23	31	4

Table 2. Best fit of the material constants for von Mises and Drucker-Prager (D-P) material models

An extension of the presented material model is visco-elasto/plastic material model with damage, described in total by 10 material constants; two elastic constants: Young's modulus E and Poisson's ratio ν, two constants describing the von Mises yield criterion with bilinear isotropic hardening: yield stress σ_y, tangent modulus E_{tan}, four constants for implicit creep C_1, C_2, C_3, C_4 with time hardening according to the equation:

$$\dot{\varepsilon}_{cr} = C_1 \sigma^{C_2} t^{C_3} e^{-C_4/T} \tag{3}$$

where $\dot{\varepsilon}_{cr}$ is the change in equivalent creep strain with respect to time, σ is the equivalent stress, t is the time at end of a substep and T is the temperature, and finally, two constants D_1, D_2 for damage model published in [37]:

$$E_{new} = (1 - d_c) E_0 \tag{4}$$

in which isotropic damage parameter d_c is defined as:

$$d_c = D_1(1 - e^{-D_2\varepsilon_{eqv}^{pl}}) \tag{5}$$

where E_{new} is the degraded Young's modulus which is calculated at the end of each loadstep, E_0 is the initial Young's modulus and ε_{pl}^{eqv} is the accumulated equivalent plastic strain at the end of loadstep. Table 3 gives overview on the material constants fitted using the whole set of nanoindentation curves for different loading rates, dwell times and maximal indentation forces.

	mean value	standard deviation
Young's modulus [GPa]	15.39	1.4
Poisson's ratio [-]	0.2[1)]	–
yield stress σ_y [MPa]	180	43
tangent modulus E_{tan} [MPa]	1854	336
C_1 [-]	3.1×10^{-18}	4.1×10^{-18}
C_2 [-]	6.1	0.42
C_3 [-]	0.88	0.71
C_4 [-]	0	–[2)]
D_1 [-]	0.73	0.037
D_2 [-]	25.3	7.48

Table 3. Best fit of the material constants for visco-elasto/plastic material model with damage. Value indicated by [1)] was expertly determined and value indicated by [2)] was not varied.

For more detailed description of fitting this material model to the whole set of nanoindentation curves as well as application of the material to modeling of deformation behavior of single trabecula see [38].

3.4. Use of modulus mapping to map mechanical properties over cross-section of individual trabeculae

As it has been pointed out in Section 2 material properties of trabecular bone can vary in the cross-section of individual trabecula. This is caused by the highly uneven distribution of mineral content as a consequence on non-uniform deposition of new bone. Nanoindentation, as a measurement tool for very local mechanical properties is able to distinguish this variation in mineral content (interstitial bone has a larger mineral content compared to the bone on the trabecular surface).

Common approach in nanoindentation of trabecular bone is to cut a block sample of the tissue and prepare a larger area to be indented. This results in uncertainty whether interstitial or superficial bone is indented and can cause problems in evaluation of the results, even when tissue from one anatomical location is used. The only study that uses nanoindentation of

individual trabeculae in their cross-sections is the study by Brennan el al. [39], however, the properties were measured only in three distinct areas (core, middle, outer) and the authors used quasi-static nanoindentation. Another option is to use a quantitative technique for mapping the elastic modulus in a larger area. Modulus mapping technique can provide highly valuable information about the elastic properties in larger area, since it is equivalent to performing a dynamic indentation test in a matrix of 256×256 points.

In their pioneering work Asif et al. [47] used modulus mapping to measure elastic properties of a carbon fiber epoxy composite. MM has been used to measure the nanoscale elastic properties of the collagen fibers, fibrils and mineral deposits in extrafibrillar space [48] in order to evaluate properties of nanocomposite films to mimic the hierarchy of natural bone. Recently the technique was used to measure the local variations in dentin and enamel in human teeth [49] but no verification with other experimental method has been done. In this part, MM was used to evaluate mechanical properties in a large area of single trabecula cross-section. Average material properties obtained with MM are compared to elastic modulae measured by quasi-static nanoindentation.

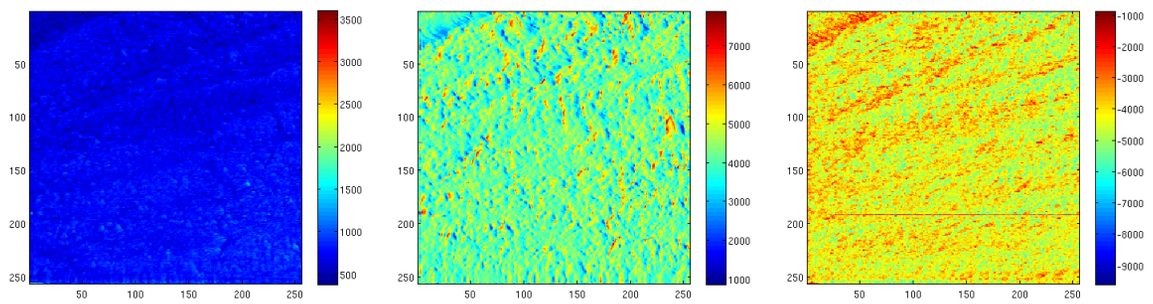

Figure 8. Exemplar image maps of (a) complex modulus, (b) loss modulus and (c) storage modulus for one indented cross-section of human trabecula

Figure 9. Cross-section of trabecula embedded in epoxy resin. Image acquired by optical microscopy.

To measure elastic properties in a larger area (35×35 μm) of trabecula's cross-section, modulus mapping technique (combination of nanoDMA and in-situ SPM) was used. In this process, the probe is sinusoidally oscillating over the polished surface with a given frequency and load. From the recorded displacement amplitude and phase lag storage and loss modulae are determined. During MM a small sinusoidal force is superimposed on top of a larger quasi-static force. Motion of the vibrating system of indenter and the surface sample can

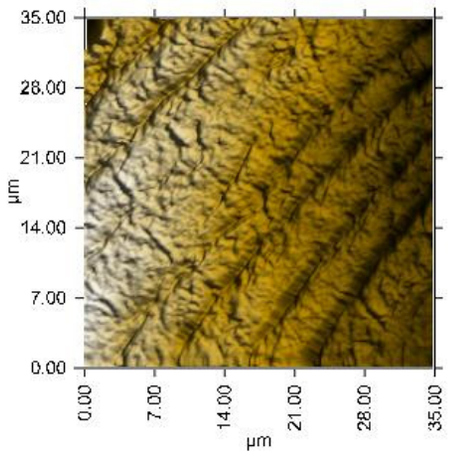

Figure 10. Typical topography of the surface sample acquired by in-situ SPM (dimensions of scanned area 35×35 µm.)

be described by equation of motion for one degree of freedom. Harmonic equation describing the motion is:

$$F_0 \sin(\omega t) = m\ddot{x} + c\dot{x} + kx \tag{6}$$

in which F_0 is the magnitude of the harmonic force, ω is the circular frequency of the system, c is the damping coefficient and k is the stiffness of the system. The system is here assumed to be linear viscoelastic. Denoting C_i stiffness of the indenter, C_s stiffness of the sample and A_0 amplitude of the system's response, we can write following equation for the time evolution of the dynamic response:

$$A_0 = \frac{F_0}{\sqrt{\left(k - m\omega^2\right)^2 + \left[\left(C_i + C_s\right)\omega\right]^2}} \tag{7}$$

Denoting $k = k_s + k_i$ (k_s is stiffness of the sample, k_i is stiffness of the indenter and k is the total spring stiffness) we can calculate the phase difference φ between the force and displacement from:

$$\tan\phi = \frac{\left(C_i + C_s\right)\omega}{k - m\omega^2} \tag{8}$$

Prior the measurement, a dynamic calibration of the system is performed to establish three parameters of the system (indenter mass m, damping coefficient of the capacitive displacement sensor C_i, stiffness of the indenter k_i), leaving only stiffness k_s and damping coefficient C_s of the sample as unknown values. In indentation, the contact stiffness k_s is proportional to the projected contact area A_c:

$$k_s = 2E^* \sqrt{\frac{A_c}{\pi}} \tag{9}$$

Using this, storage modulus $E^{'}$, loss modulus $E^{''}$ and phase shift between the force and displacement δ can be calculated using following equations:

$$E^{'} = \frac{k_s\sqrt{\pi}}{2\sqrt{A_c}},\ E^{''} = \frac{\omega C_s\sqrt{\pi}}{2\sqrt{A_c}},\ \tan\delta = \frac{\omega C_s}{k_s} \tag{10}$$

From the storage and loss modulae, complex modulus E^* can be computed using:

$$E^* = E^{'} + iE^{''} \tag{11}$$

As a result of the MM technique, the stiffness is continuously measured in the pixel matrix and the modulus includes the real and imaginary part providing the storage ($E^{'}$) and loss ($E^{''}$) modulae of the material.

3.5. Comparison with quasi-static nanoindentation

In our experiments, the 256×256 square matrix represented physical area 35×35 µm. In each point of the matrix storage and loss modulae were evaluated. To compare results from MM technique with quasi-static indentation, each sample was indented with a set of 9 indents in the center of the area used for MM. In quasi-static indentation, maximal force 1000 µN was applied in 5 s loading part, which was followed by 5 s holding part, finished with 5 s unloading part.

Modulus mapping shows the trend of larger stiffness in core, smaller values are measured in superficial areas. Both quasi-static nanoindentation and MM can be used to measure the elastic properties of extracted trabeculae, however, to identify material constants for more complex material model (e.g. von Mises plasticity with kinematic hardening) it is necessary to use different experimental program, e.g. nanoindentation with various strain rates or micromechanical testing as will be described in the following chapter.

4. Micromechanical testing of isolated trabeculae

Apart from nanoindentation, delicate tensile or bending tests can be performed with extracted trabeculae. The most important advantage of micromechanical testing is that it is well-developed and straightforwad technique. Moreover, using mechanical testing it is possible not only to measure the Young's modulus, but also yield properties or properties at different strain rates can be assessed. In this section a method for measuring elastic modulus and yield stress using micromechanical testing of individual trabeculae will be described in detail.

4.1. Shape from silhouettes

The difficulty of performing mechanical tests with samples of such small dimensions (diameter of an average human trabecula from proximal femur is about 100 µm) lies not only in complicated manipulation with the samples, but also in precision of the measurement. The dimensions of the samples must be measured with micrometer precision and due to the irregularity in the samples' shape it is necessary to measure the real shape of each sample. To assess the precise shape of the trabeculae, every sample can be scanned in a micro-CT device (resolution of 1-5 µm is needed) and its geometry reconstructed with filtered backprojection for the cone beam scanning geometry.

Another option is to reconstruct the 3-D shape of the sample from its silhouettes. This is a method commonly used to obtain 3-D shapes from silhouettes captured by multiple cameras with the volume intersection method. The problem is stated as follows: Given a set of calibrated images of an object taken from different angles can we reconstruct its 3-D

model? The simplest method to perform this reconstruction is to use the so called *visual hull* which is the shape maximally consistent with the silhouettes. The visual hull is the intersection of the silhouette cones produced by images taken from different viewpoints (see Fig. 11). It can be easily shown that the visual hull cannot capture concavities not visible in the silhouettes which can lead to reconstruction artifacts such as erroneous additional connected components. In the reconstruction, the foreground object is separated from the background by binary thresholding and silhouette image is this binary foreground/background image.

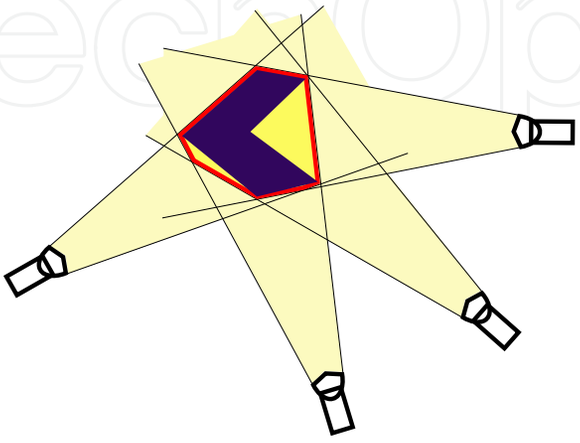

Figure 11. The principle of visual hull. It is the intersection of silhouette cones (green), which is a bounding geometry of the object

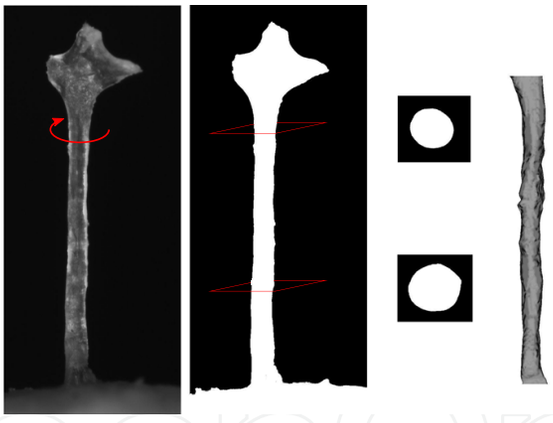

Figure 12. Reconstruction of the geometry of extracted trabeculae. Only middle part of the sample (between the supports) is needed.

It can be shown that for convex objects the reconstruction from images converges to the true shape as more view angles are added. This technique has been used in our experiments with isolated trabeculae. Prior the testing, each sample was mounted on a rotational stage driven by stepper motor and its shade was captured with a CCD camera attached to a microscope. The sample was rotated by 360° in 1° increments and its silhouettes captured with the camera. From the shade images the real geometry of each sample was reconstructed with error less than 4%.

The geometry of the trabecula is represented by its surface given as a set of connected triangles (see Fig. 12). The volume of the sample is discretized with tetrahedral elements using a constrained Delaunay approach [50]. After shape optimization of the tetrahedral elements,

mid-side nodes are added for more accurately calculated gradients in deflections, strains and stresses in all FE calculations.

4.2. Displacement tracking using DIC

To measure the applied load and displacements with high accuracy a novel experimental device (Fig. 13) has been developed which enables to control the displacement of the loading tip with sub-micron positioning capability by means of differential micrometer with 0.1 µm sensitivity. Positioning of the supports and the sample is provided by precision double-row ball bearing linear stages with 1 µm sensitivity. This very high accuracy in positioning is necessary for perfect loading and exact geometry of the experimental setup (see the close-up view in Fig. 15a and Fig. 15b).

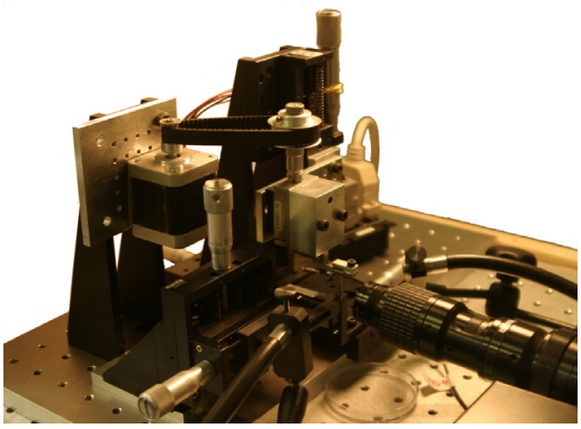

Figure 13. Experimental setup for the optical measurement of extracted trabecula in three-point bending.

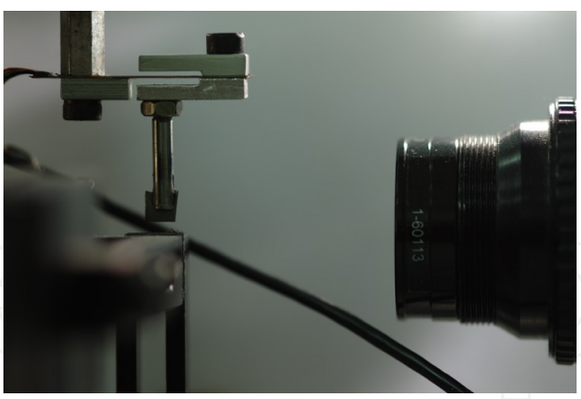

Figure 14. Close-up view of the sample showing the loading tip attached to the miniature load cell. High magnification (12×) lens on right.

The deformation of the sample is measured optically using a high-resolution CCD camera. The strain field is evaluated with an image correlation algorithm [51] applied to the part of the sample between the supports.

DIC is based on the maximization of a correlation coefficient that is computed in subsets of the image surrounding the measurement points. Correlation between the pixel intensity in the image subsets between two corresponding images (at time t_i and t_{i+1}) is computed for every

measured point with a non-linear optimization technique (inverse compositional algorithm). Coefficients of the affine transformation between the deformed and original position are used to compute the deformation gradient tensor F. Green-Lagrange deformation tensor is then computed from: $E = \frac{1}{2}(F^T F - I)$.

In the bending tests, only displacements are evaluated with DIC. The displacements are used to find the best fit between the experimental results and results computed using FE simulation of the bending test with real geometry of the sample. This procedure is described in the following text.

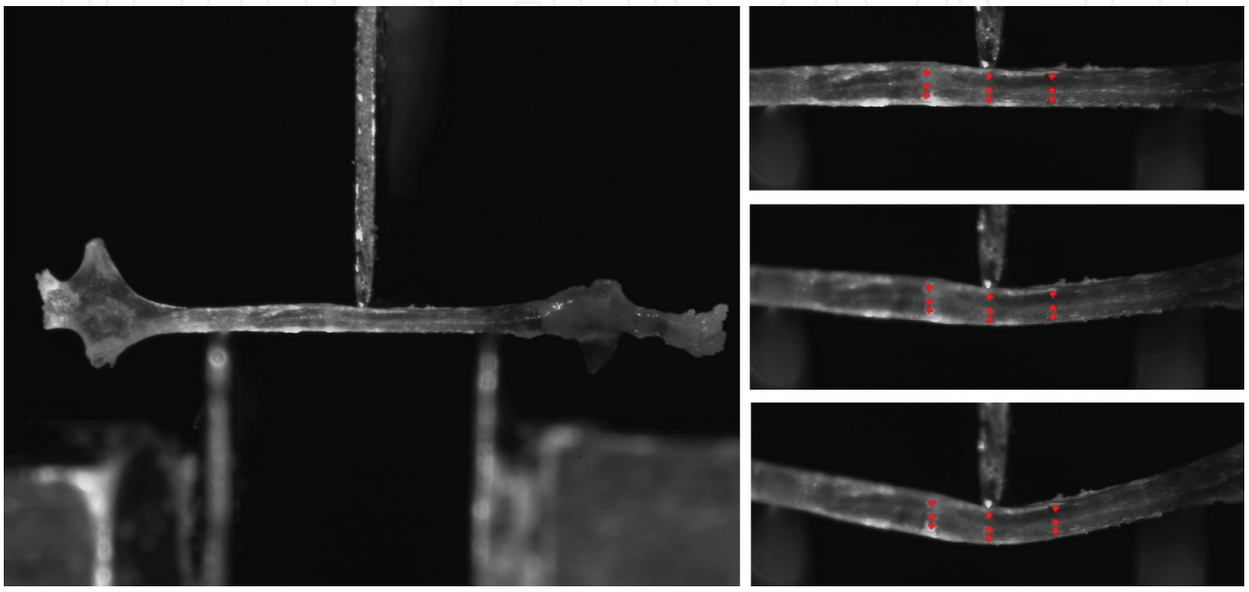

a) *b)*

Figure 15. Three-point bending of isolated trabecula. Straight sample resting on supports with span length equal to 1 mm (a). Principle of tracking "markers" on the sample using DIC (b).

4.3. Results from 3-point bending

To account for the real geometry of each irregularly shaped specimen, FE model reflecting the true geometry is developed using the shape-from-silhouettes approach. Exact position of the supports and the loading tip is established from the high-resolution images. Boundary conditions and loading of the FE model are prescribed to match exactly the experimental conditions for each sample. Using similar fitting procedure as described for the FE model of nanoindentation a set of material parameters is determined to find the best fit between the experimental force–displacement curves and those determined from the numerical simulation.

Because the displacements are actually measured in three distinct locations (using the image correlation), the same positions are determined in the FE model and displacements in each load increment are calculated in these points. Values from the FE simulation are compared to the measured values. Example of the best-fit for selected “markers” in the FE model are depicted (together with displacement field in the model) in Fig. 16.

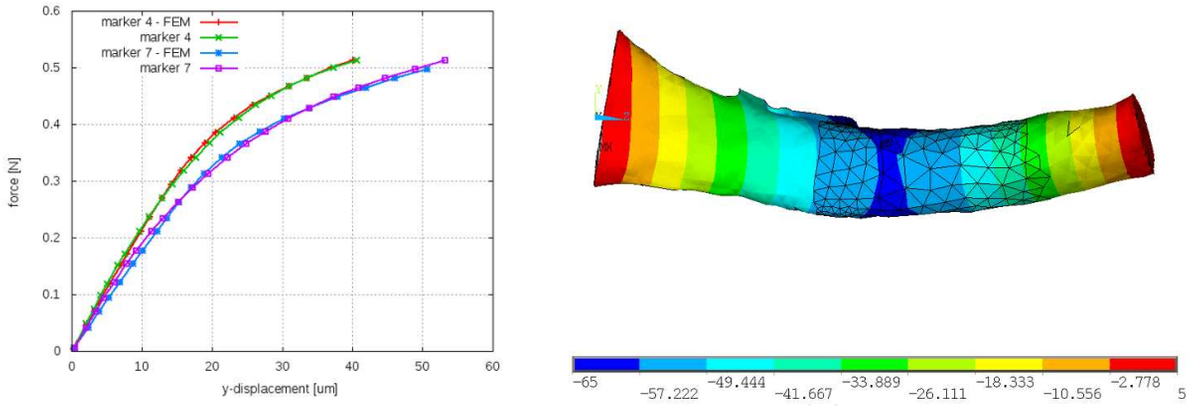

Figure 16. Example of fitting the force-deflection curves calculated by the FE model to experimentally determined ones (left). Only part of the sample between the supports is considered by the FE model of the specimen's real geometry(right).

4.4. Results from micromechanical testing compared to nanoindentation

To compare nanoindentation with micromechanical testing, only the elastic properties were determined by the two different methods. For the nanoindentation, only parts of the trabeculae outside the supports were used. In this region, the bending moment is zero and this part of the sample can be considered undamaged. After the bending test, each sample was embedded in the upright position in the low shrinkage epoxy resin and polished to reveal the cross-section close to one of the ends of trabecula. After surface polishing the nanoindentation experiments described in section 3 were undertaken. Elastic properties obtained from nanoindentation and those assessed by the micromechanical bending tests are compared in Tab. 4.

sample No.	quasi-static nanoindentation [GPa]	bending test [GPa]
1	12.04	11.07
2	15.93	13.26
3	16.22	13.87
4	17.82	14.52
5	17.91	14.70
6	12.07	10.51

Table 4. Average values of elastic modulae obtained by quasi-static indentation in the cross-section of each trabecula compared to the results of micromechanical tests with single trabecula (three-point bending)

From Tab. 4 it is clear, that both methods give very similar results in terms of elastic properties. The values of elastic modulus measured by three-point bending are 10% - 20% lower that those assessed by nanoindentation. This can be explained by the fact that nanoindentation is not performed in the very outer part of the cross-section, thus giving more information about the core hardness, which is stiffer. Another reason might be in overestimation of

the cross-sectional area by the shape-from-silhouettes method. The overestimation of the cross-sectional area is well under 3%, however, the calculation of bending stiffness can lead to overestimation over 5%.

5. Application to constitutive modeling of trabecular bone tissue

The importance of assessment of mechanical properties at the tissue level, i.e. at the level of single trabeculae can be demonstrated using indirect determination of trabecular bone mechanical properties from high-resolution images of its internal architecture. These micro-FE models, i.e. models properly describing the geometry of the trabecular bone architecture are nowadays a common tool for assessment of mechanical properties of trabecular bone [52]. The high-resolution images can be obtained from micro-CT images, peripheral quantitative computed tomography (pQCT) or, more recently with high-resolution magnetic resonance (MR) imaging.

These models can be used to study the relation between the microstructure, material properties at the tissue level and overall mechanical properties. It can be used to predict evolution of mechanical properties with osteoporotic changes to the microstructure and thus to assess evolution of osteoporotic fracture risk. Moreover, combined with experimental tests with small-scale samples of trabecular bone, these models can be used to verify the tissue constitutive models. This can be achieved by comparing the response of micro-FE model with the response of the real sample.

Additionally, microtomographic scanning of a sample can be performed in a time-lapse fashion, i.e. a sequence of a time-lapse micro-CT [53] of the specimen under gradually incremented load is performed and the deformed microstructure is recorded. A custom, laboratory micro-radiographic system composed of micro-focus X-ray tube and a large flat panel detector [54] can be used for such an experiment. Reconstruction of the internal structure is provided using backprojection algorithm for equiangular cone-beam projection data [55] for each load increment.

To compare the strains in the loaded sample to the values calculated by the FE analysis a Digital Volume Correlation (DVC) [56, 57] method is used. DVC can be seen as a natural extension of existing digital image correlation techniques [59] to three dimensions. Example of a comparison between the experimentally measured strain distribution in a loaded sample and numerical simulation can be found in [58].

The bone microstructure can be discretized using a tetrahedral mesh. In the nodal points of the mesh the displacement vector is computed using X-ray digital volumetric correlation technique. For each of the tetrahedral element the Green-Lagrange strain tensor is calculated from the displacements of its vertices. The overlaid tetrahedral mesh serves not only for the calculation of the deformation tensor, but also for easy visualization of the vector and tensor fields and for fast and direct comparison with results of numerical simulations. The numerical simulations can use the existing tetrahedral mesh or the mesh can be easily refined/coarsened if needed. Illustrative example of the FE model and displacement field computed with DIC is shown in Fig. 18.

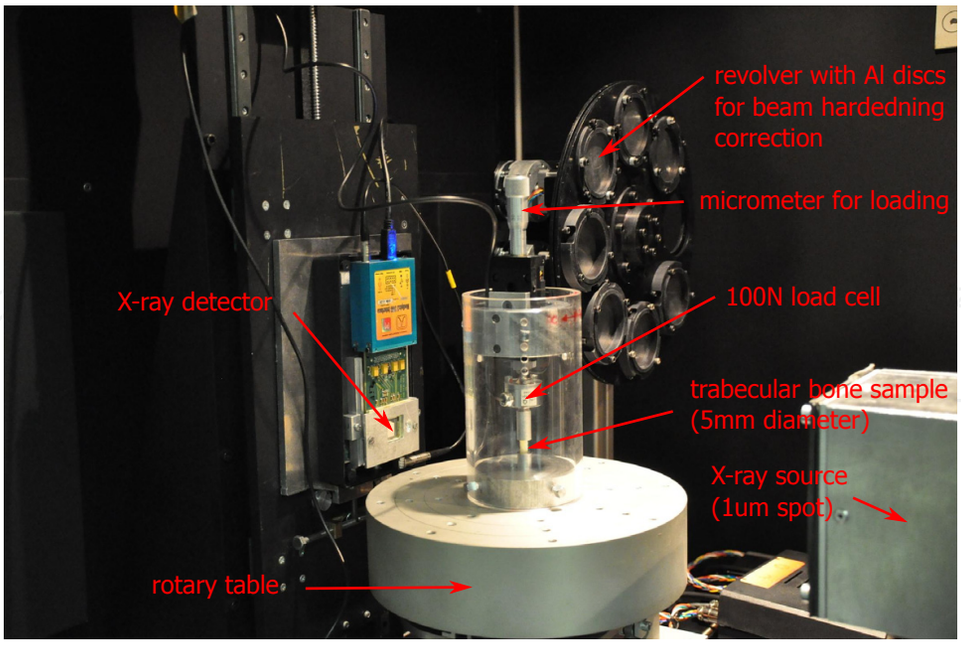

Figure 17. Experimental setup for time-lapse X-ray rentgenography. Sample is tested in three-point bending and X-ray projections of the deformed state are captured using exposures with very small time (250 ms)

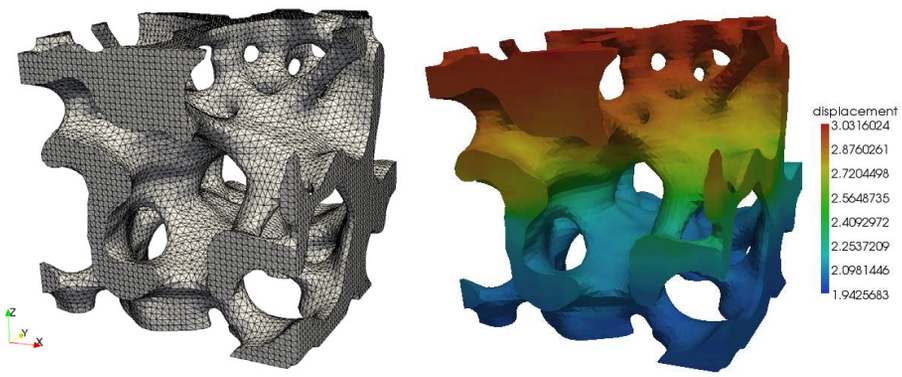

Figure 18. Small part of the micro-FE model of trabecular bone. FE mesh of the model (a) and displacement field (b). Illustrative image.

6. Conclusions

An overview of techniques used to determine material properties of trabecular bone at different microstructural levels was presented in the chapter. The focus was paid on two important methods for measurement of mechanical properties at the tissue level: i) nanoindentation and ii) micromechanical testing. In the part focused on nanoindentation two methods, i.e. quasi-static indentation and modulus mapping were compared. Apart from measurement of the elastic properties, a method based on fitting the response of FE model of indentation to experimental curves was introduced.

Apart from nanoindentation, another approach to measure material properties of trabeculae was described. This approach is based on precise micromechanical tests performed with individual trabeculae. A methodology how to account for the imperfect shape of the

small-scale specimens was introduced. This methodology is based on developing exact FE model of each tested specimen using the shape-from-silhouettes approach. Discussion of precision of the measurements as well as precision of the geometry reconstruction was shortly given.

In the last part of the chapter, application of the tissue material properties to modeling of trabecular bone was given. Short description of the development process of micro-FE models, i.e. FE models of the trabecular micro-architecture was described and utilization of microfocus Computed Tomography or other high-resolution imaging methods was outlined.

Precise and reliable measurement of tissue mechanical properties of trabecular bone as a key factor for the overall bone strength is important not only for reliable assessment of osteoporotic fracture risk assessment but also for precise evaluation of the effects of treatment procedures, e.g. in animal studies. Although the term bone quality is poorly defined, it is clear that current diagnostic techniques for measuring the bone quality in vivo do not yield reliable results. To improve the current diagnostic methods all the influencing factors, i.e. tissue properties, geometric, microarchitectural and connectivity factors, must be taken into account and a combination of all described methods must be used.

Acknowledgements

Support of the Czech Science Foundation (P105/10/2305) is gratefully acknowledged.

Author details

Ondřej Jiroušek
Institute of Theoretical and Applied Mechanics
Academy of Sciences of the Czech Republic, v.v.i.,
Prague, Czech Republic

7. References

[1] Birkenhager-Frenkel DH, Nigg AL, Hens CJJ, Birkenhager JC. Changes of interstitial bone thickness with age in men and women. Bone 1993; 14(3) 211-216.
[2] Boyde A, Elliott JC, Jones SJ. Stereology and histogram analysis of backscattered electron images: Age changes in bone. Bone 1993; 14(3) 205-210.
[3] van der Linden JC, Birkenhager-Frenkel DH, Verhaar JAN, Weinans H. Trabecular bone's mechanical properties are affected by its non-uniform mineral distribution. Journal of Biomechanics 2001; 34(12) 1573-1580.
[4] Parfitt AM. The composition, structure and remodeling of bone a basis for the interpretation of bonemineral measurements. In: Dequeker J, Geusens P, Wahner HW. (eds.) Bone Mineral Measurements by Photon Absorptiometry: Methodological Problems, 1988; Leuven University Press, Leuven, 9-28.
[5] Petersen MM, Gehrchen PM, Nielsen PK, Lund B. Loss of bone mineral of the hip assessed by DEXA following tibial shaft fractures. Bone 1997; 20(5), 491-495.

[6] Pafumi C, Chiarenza M, Zizza G. Role of DEXA and ultrasonometry in the evaluation of osteoporotic risk in postmenopausal women. Maturitas 2002; 42 113-117.
[7] Cummings SR, Bates D, Black DM. Clinical use of bone densitometry: scientific review. JAMA 2002; 288 1889-1897.
[8] Silva MJ, Gibson LJ. Modeling the mechanical behavior of vertebral trabecular bone: Effects of age-related changes in microstructure. Bone 1997; 21(2) 191-199.
[9] Sievanen H, Weynand LS, Wacker WK, Simonelli C, Burke PK, Ragi S, Del Rio L. A Novel DXA-Based Hip Failure Index Captures Hip Fragility Independent of BMD. Journal of Clinical Densitometry 2008; 11(3) 367-372.
[10] Wren TAL, Liu X, Pitukcheewanont P, Gilsanz V. Bone Densitometry in Pediatric Populations: Discrepancies in the Diagnosis of Osteoporosis by DXA and CT. The Journal of Pediatrics 2005; 146(6) 776-779.
[11] Carte DR, Hayes WC. The compressive behavior of bone as a two-phase porous structure. Journal of Bone and Joint Surgery - Series A 1977; 59 (7) 954-962.
[12] Goldstein SA. The mechanical properties of trabecular bone: Dependence on anatomic location and function. Journal of Biomechanics 1987; 20 (11-12) 1055-1061.
[13] Deligianni DD, Maris A, Missirlis YF. Stress relaxation behaviour of trabecular bone specimens. Journal of Biomechanics 1994; 27 (12) 1469-1476.
[14] van Rietbergen B, Odgaard A, Kabel J, Huiskes R. Direct mechanics assessment of elastic symmetries and properties of trabecular bone architecture. Journal of Biomechanics 1996; 29 (12) 1653-1657.
[15] Wolfram U, Wilkea H, Zysset PK. Transverse isotropic elastic properties of vertebral trabecular bone matrix measured using microindentation (effects of age, gender and vertebral level). Bone 2009; 44 S392–S393.
[16] Reisinger AG, Pahr DH, Zysset PK. Principal stiffness orientation and degree of anisotropy of human osteons based on nanoindentation in three distinct planes Journal of the Mechanical Behavior of Biomedical Materials 2011; 4 (8) 2113-2127.
[17] Yamashita J, Li X, Furman BR, Rawls HR, Wang X, Agrawal CM. Collagen and bone viscoelasticity: A dynamic mechanical analysis. Journal of Biomedical Materials Research 2002; 63 (1) 31-36.
[18] Wang X, Bank RA, Tekoppele JM and Agrawal CM. The role of collagen in determining bone mechanical properties. Journal of Orthopaedic Research 2001; 19 1021–1026.
[19] Bembey AK, Bushby AJ, Boyde A, Ferguson VL, Oyen ML. Hydration effects on the micro-mechanical properties of bone. Journal of Materials Research 2006; 21(8) 1962-1968.
[20] Broz JJ, Simske SJ, Greenberg AR, Luttges MW. Effects of rehydration state on the flexural properties of whole mouse long bones. Journal of Biomechanical Engineering 1993; 115 (4 A) 447-449.
[21] Bembey AK, Oyen ML, Bushby AJ, Boyde A. Viscoelastic properties of bone as a function of hydration state determined by nanoindentation. Philosophical Magazine 2006; 86 (33-35) 5691-5703.
[22] Oliver WC and Pharr GM. An improved technique for determining hardness and elastic modulus using load and displacement sensing indentation experiments. Journal of Materials Research 1992; 7(6) 1564-1583.

[23] Pharr GM. Measurement of mechanical properties by ultra-low load indentation. Materials Science and Engineering A 1998; 253(1-2) 151-159.
[24] Pharr GM, Oliver WC, Brotzen FR. On the generality of the relationship among contact stiffness, contact area, and the elastic modulus during indentation. Journal of Materials Research 1992; 7(3) 613–617.
[25] Dumas G, Baronet CN. Elastoplastic indentation of a half-space by an infinitely long rigid circular cylinder. International Journal of Mechanical Sciences 1971; 13 (6) 519-530.
[26] Hardy C, Baronet CN, Tordion GV. Indentation of an elastic-perfectly-plastic half-space by a hard sphere. Journal of Basic Engineering 1972; 94(1) 251-253.
[27] Cheng YT, Cheng CM. Scaling Relationships in Conical Indentation of Elastic Perfectly Plastic Solids. International Journal of Solids Structures 1999; 36 1231–1243.
[28] Wang X, Allen MR, Burr DB, Lavernia EJ, Jeremic B, Fyhrie DP. Identification of material parameters based on Mohr–Coulomb failure criterion for bisphosphonate treated canine vertebral cancellous bone. Bone 2008; 43 (4) 775-780.
[29] Jiroušek, O., Nemecek, J., Kytýr, D., Kunecký, J., Zlámal, P., Doktor, T., Nanoindentation of trabecular bone-comparison with uniaxial testing of single trabecula. Chemicke Listy 2011; 105 (17) s668-s671.
[30] Rho JY, Tsui TY, Pharr GM. Elastic properties of human cortical and trabecular lamellar bone measured by nanoindentation. Biomaterials 1997; 18(20) 1325-1330.
[31] Zysset PK, Guo XE, Hoffler CE, Moore KE, Goldstein SA. Elastic modulus and hardness of cortical and trabecular bone lamellae measured by nanoindentation in the human femur. Journal of Biomechanics 1999; 32(10) 1005-1012.
[32] Turner CH, Rho J, Takano Y, Tsui TY, Pharr GM. The elastic properties of trabecular and cortical bone tissues are similar: Results from two microscopic measurement techniques. Journal of Biomechanics 1999; 32(4) 437-441.
[33] Rho JY, Roy ME 2nd, Tsui TY, Pharr GM. Elastic properties of microstructural components of human bone tissue as measured by nanoindentation. Journal of Biomedical Materials Research 1999; 45(1) 48-54.
[34] Hoffler CE, Moore KE, Kozloff K, Zysset PK, Brown MB, Goldstein SA. Heterogeneity of bone lamellar-level elastic moduli. Bone 2000; 26(6) 603-609.
[35] Hengsberger S, Kulik A, Zysset P. Nanoindentation discriminates the elastic properties of individual human bone lamellae under dry and physiological conditions. Bone 2002; 30(1) 178-184.
[36] Roschger P, Paschalis EP, Fratzl P, Klaushofer K. Bone mineralization density distribution in health and disease. Bone 2008; 42(3) 456-466.
[37] Zhang J, Michalenko MM, Kuhl E. Characterization of indentation response and stiffness reduction of bone using a continuum damage model. Journal of the mechanical behavior of biomedical materials 2010; 3(2), 189-202.
[38] Zlámal P, Jiroušek O, Kytýr D, Doktor T. Indirect determination of material modelparameters for single trabecula based o nanoindentation and three-point bending test. Proceedings of the 18^{th} international conference Engineering Mechanics 2012; 1 394-395.
[39] Brennan O, Kennedy OD, Lee TC, Rackard SM, O'Brien FO Biomechanical properties across trabeculae from the proximal femur of normal and ovariectomised sheep. Journal of Biomechanics 2009; 42(4) 498-503.

[40] Jiroušek O, Kytýr D, Zlámal P, Doktor T, Šepitka J, Lukeš J. Use of modulus mapping technique to investigate cross-sectional material properties of extracted single human trabeculae. Chemické Listy 2012; accepted.
[41] Dudíková M, Kytýr D, Doktor T, Jiroušek O. Monitoring of material surface polishing procedure using confocal microscope. Chemické Listy 2011; 105(17) 790-791.
[42] Tang B and Ngan AHW. Accurate measurement of tip–sample contact size during nanoindentation of viscoelastic materials. Journal of Materials Research 2003; 18 1141-1148.
[43] Oyen ML, Cook RF. A practical guide for analysis of nanoindentation data. Journal of the Mechanical Behavior of Biomedical Materials 2009; 2(4) 396-407.
[44] Nemecek J. Creep effects in nanoindentation of hydrated phases of cement pastes. Materials Characterization 2009; 60(9) 1028–1034.
[45] Mencík J, He LH, Nemecek J. Characterization of viscoelastic-plastic properties of solid polymers by instrumented indentation. Polymer Testing 2011; 30 101–109.
[46] Sneddon IN. The relation between load and penetration in the axisymmetric Boussinesq problem for a punch of arbitrary profile. International Journal of Engineering Science 1965; 3(1) 47-57.
[47] Asif SA, Wahl KJ, Colton RJ, Warren OL. Quantitative imaging of nanoscale mechanical properties using hybrid nanoindentation and force modulation. Journal of Applied Physics 2001; 90(3) 1192-1200.
[48] Khanna R, Katti SK, Katti DR. Bone Nodules on Chitosan-Polygalacturonic Acid-Hydroxyapatite Nanocomposite Films Mimic Hierarchy of Natural Bone. Acta Biomaterialia 2011; 7 1173-1183.
[49] Balooch G, Marshall GW, Marshall SJ, Warren OL, Asif SAS, Balooch M. Evaluation of a new modulus mapping technique to investigate microstructural features of human teeth. Journal of Biomechanics 2004; 37 1223-1232.
[50] Edelsbrunner H and Shah NR. Incremental Topological Flipping Works for Regular Triangulations. Algorithmica 1996; 15 223-241.
[51] Jandejsek I, Valach J, Vavrík D. Optimization and Calibration of Digital Image Correlation Method. In Experimentální analýza napetí 2010. Olomouc: Univerzita Palackého v Olomouci, 121-126.
[52] Verhulp E, van Rietbergen B, Müller R, Huiskes R. Indirect determination of trabecular bone effective tissue failure properties using micro-FE simulations. Journal of Biomechanics 2008; 41(7) 1479-1485.
[53] Nazarian A. and Müller R. Time-lapsed microstructural imaging of bone failure behavior. Journal of Biomechanics 2004; 37(1) 55-65.
[54] Jakubek J, Holy T, Jakubek M, Vavrik D, Vykydal Z. Experimental system for high resolution X-ray transmission radiography. Nuclear Instruments and Methods in Physics Research Section A: Accelerators, Spectrometers, Detectors and Associated Equipment 2006; 563(1), 278-281.
[55] Vavrík D, Soukup P. Metal grain structure resolved with table-top micro-tomographic system. Journal of Instrumentation 2011; 6 (11), art. no. C11034.
[56] Jiroušek O, Jandejsek I, Vavrík D. Evaluation of strain field in microstructures using micro-CT and digital volume correlation. Journal of Instrumentation 2011; 6 (1), art. no. C01039.

[57] Jandejsek I, Jiroušek O, Vavrík D. Precise strain measurement in complex materials using digital volumetric correlation and time lapse micro-CT data. Procedia Engineering 2011; 10(1) 1730-1735.

[58] Jiroušek O, Zlámal P, Kytýr D, Kroupa M. Strain analysis of trabecular bone using time-resolved X-ray microtomography. Nuclear Instruments and Methods in Physics Research, Section A: Accelerators, Spectrometers, Detectors and Associated Equipment 2011; 633 (SUPPL. 1) S148-S151.

[59] Lucas BD and Kanade T. An iterative image registration technique with an application to stereo vision. Proceedings of the 1981 DARPA Image Understanding Workshop, April, 1981 121-130.